Supporting Information

Jeoung and Dobbek 10.1073/pnas.1720489115

SI Materials and Methods

Anoxic Preparations and Experiments. Anoxic solutions were prepared in a stoppered bottle/tube with a screw cap with butyl rubber septum by successive cycles of evacuating and N_2 gas flushing at a Schlenk line.

All experiments unless described were carried out under anoxic conditions inside a glove box (model B; COY Laboratory Products) under an atmosphere of 95% N_2/5% H_2 (Air-Liquide GmbH).

Cloning, Expression, and Purification. Genes *CHY*_0487 and *CHY*_0488, annotated as a dehydratase family protein (named $DCCP_{Ch}$ in this work) and a putative CoA-substrate-specific activase (named DCCP-R_{Ch} in this work), respectively, were amplified from the genomic DNA of *Carboxydothermus hydrogenoformans* Z-2901 by PCR with Phusion DNA polymerase using different primer sets as listed: *Fw_DCCP-17*, 5′-gcatcgggtctcg-gcgccgacaatcgggagttg-tggaag-3′; *Rv_DCCP-17*, 5′-gcatcgggtctcgtatcactactttatcatctccaa-aaag-3′; *Fw_DCCP-28-His*, 5′-cagccatatggacaatcgggagttgtggaag-3′; *Rv_DCCP-28-His*, 5′-gcactcgagctactttatc-atctccaaaaag-3′; *Fw_DCCPR-IBA3*, 5′-ggagatggtctcgaatgtttgcaggattagatttg-3′; *Rv_DCCPR-IBA3*, 5′-ggagatggtctcggcgctactcccggtttctctggcaattaaag-3′.

An approximately 1.3-kbp PCR product for *CHY*_0487 using a primer set of either Fw/Rv_DCCP-17 for pASK-IBA17(+) or Fw/Rv_DCCP-28-His for pET28a-His-TEV was digested by BsaI and NdeI/XhoI to ligate into a BsaI-digested pASK-IBA17(+) vector and NdeI/XhoI-digested pET28a-His-TEV vector that was modified with a tobacco etch virus (TEV) cleavage site between N-terminal His-tag and the start methionine. The resulting plasmids were named pCHX-IBA17 and pCHX-28HTEV, respectively. A PCR-amplified 0.74-kbp product for the *CHY*_0488 using a primer set of Fw/Rv_DCCPR-IBA3 was digested by BsaI, which was introduced to a BsaI-restricted pASK-IBA3. The positive plasmid was named pCHXR-IBA3. All plasmids cloned in this work were checked by DNA sequencing (Eurofins MWG Operon). The quick-change method was used to exchange single amino acids of the $DCCP_{Ch}$ ($C^{94}A$ and $K^{146}A$) with the pCHX-28HTEV as a template using *Pfu* DNA polymerase (Fermentas), named pCHX-28HTEV-C94A and pCHX-28HTEV-K146A.

The plasmids pCHX-IBA17, pCHX-28HTEV-C94A, and pCHX-28HTEV-K146A were transformed into *Escherichia coli* Rosetta(DE3) with pRKISC (1). The resulting strains were cultivated anaerobically in a 5-L bottle completed with TB media containing 100 μg/mL tetracycline together with 50 μg/mL carbenicillin for pCHX-IBA17 and 50 μg/mL kanamycin for pCHX-28HTEV-C94A and -K146A at room temperature (approximately 22 °C). When the culture reached around 0.6 of OD_{600}, addition of 0.2 μM anhydrotetracycline (AHT) for the strain with pCHX-IBA17 and 0.5 mM isopropyl-β-D-thiogalactopyranoside (IPTG) for the strains with pCHX-28HTEV-C94A and -K146A initiated expression of the wild-type and the variants of $DCCP_{Ch}$. The plasmid pCHXR-IBA3 was introduced into the *E. coli* BL21 (DE3) strain, which was cultivated anaerobically in a 5-L bottle completed with TB media containing 1% (wt/vol) glucose and 50 μg/mL carbenicillin at room temperature. When the culture reached around 0.4 of OD_{600}, expression of DCCP-R_{Ch} was initiated by addition of 0.2 μM AHT. All cultures were harvested at 20 h after induction. Cell pellets were quickly frozen in liquid nitrogen and kept at −80 °C.

For purifications of proteins expressed with the strep-tag, frozen cell pastes were suspended in 50 mL buffer A (50 mM Mops pH 7.2) containing 300 mM KCl, 1 mM DT and 2 mM DTT supplemented with a pinch of avidin. Cells were broken by sonication (Branson sonifier) in a glass rosette on ice. After centrifugation at 185,667 × *g* for 1 h, the supernatant was applied to a strep-tactin Sepharose superflow column (15 mL) equilibrated in buffer A. Protein was eluted with buffer A containing 2.5 mM desthiobiotin. In the purification of DCCP-R_{Ch}, 1 mM ADP and 10 mM $MgCl_2$ were additionally added to the cell suspension and elution buffers. The affinity purified $DCCP_{Ch}$ was buffered into buffer A containing 1 mM DT and 2 mM DTT by using a PD10 column, while the eluent of DCCP-R_{Ch} was directly concentrated without buffer exchange. Buffer-exchanged $DCCP_{Ch}$ was incubated for 12 h with strep-tagged TEV protease at room temperature. During reloading of the TEV-treated $DCCP_{Ch}$ samples, the flow-through fraction was collected for enrichment of tag-free $DCCP_{Ch}$ proteins. $DCCP_{Ch}$ was finally buffered to 20 mM Tris·HCl pH 8.0 containing 1 mM DT and 2 mM DTT using a PD10 column.

To purify the two variants of $DCCP_{Ch}$, the supernatant containing the corresponding variant was loaded on a Ni-charged agarose column (10 mL) equilibrated in buffer B (50 mM Tris·HCl pH 8.0 and 1 mM DT). The $DCCP_{Ch}$ variant was eluted using buffer B containing 250 mM imidazole. After buffer exchange to buffer B by a PD10 column, the His-tag was removed by overnight incubation with His-tagged TEV protease at room temperature. To separate tag-free $DCCP_{Ch}$ variant, the solution was loaded on the Ni-agarose column, the flow-through fraction was collected, concentrated and buffer exchanged in 20 mM Tris·HCl pH 8.0 containing 1 mM DT and 2 mM DTT using a PD10 column.

Protein concentrations were routinely measured after Bradford (2) using the commercial Bio-Rad solution (Bio-Rad Laboratories).

Analytic Size-Exclusion Chromatography. Molecular weight of $DCCP_{Ch}$ in solution was determined using a superdex 200 prep-grade column (10 mm × 300 mm) equilibrated in a running buffer (50 mM Tris·HCl, pH 8.0). Approximately 200 μM isolated $DCCP_{Ch}$ was injected into the size-exclusion column. Molecular weight was calculated using a calibration curve generated from known standard proteins in the running buffer: 2 mg/mL alcohol dehydrogenase (150 kDa), 2 mg/mL albumin (66 kDa), 2 mg/mL carbonic anhydrase (29 kDa), and 2 mg/mL ribonuclease (13.7 kDa).

Network Analysis. InterPro entry of IPR010327 was analyzed using the EFI-EST server (3) with an alignment score of 20, in which edges (lines) represents BLASTP E values of $<10^{-20}$. The network is a 75% representative node network. A total 1,436 nodes were isolated from 4,978 proteins in IPR010327, visualized by Cytoscape (v3.3.0) (4) and colored by protein length (color code at the bottom). Only sequences longer than 300 aa were analyzed.

UV-Vis Spectrophotometer. UV-vis spectra were recorded using an Agilent 8453 UV-visible photodiode array spectrophotometer equipped with a Peltier cuvette thermostate (Agilent Technologies) at 25 °C inside a COY glove box. For oxidized spectra of $DCCP_{Ch}$ and DCCP-R_{Ch}, the as-isolated protein was oxidized by incubation with 200 μM thionin for 5 min and subsequently buffer-exchanged using a PD-10 column to 50 mM Hepes-NaOH pH 8.0. The thionin-oxidized 6 μM $DCCP_{Ch}$ was treated with excess addition of 2 mM DT and 1 mM Ti(III)-citrate to obtain spectra of the reduced protein. The thionin-oxidized 28 μM DCCP-R_{Ch} were reduced by addition of 0.2 mM DT.

ATPase Activity. The hydrolysis of ATP catalyzed by DCCP-R_{Ch} was determined under anoxic conditions by measuring the amount of inorganic phosphate (P_i) released during the reaction based on the malachite green assay (5). Reaction solution (1 mL) contains 12 μM DCCP-R_{Ch} with 2 mM DT in 50 mM Hepes-NaOH, pH 8.0. ATP hydrolysis was initiated by addition of 3 mM ATP/6 mM $MgCl_2$ and monitored at 35 °C. Aliquots of 5 μL were taken during the time course of reaction and absorbance at 630 nm was measured to detect the formation of a phosphomolybdate–malachite green complex. A standard curve prepared by KH_2PO_4 was used to calculate the amount of P_i released during ATP hydrolysis. To determine the influence of $DCCP_{Ch}$ and C_2H_2 on ATP hydrolysis, 4 μM $DCCP_{Ch}$ and 50% (vol/vol) C_2H_2 in 6 mL gas atmosphere were added to the activity assay.

ATP-Dependent Reduction of $DCCP_{Ch}$ by DCCP-R_{Ch}. ATP-dependent reduction of $DCCP_{Ch}$ by DCCP-R_{Ch} was determined anoxically at 25 °C. Prereduction of DCCP-R_{Ch} was achieved by adding 2 mM DT.

The assay mixture contained 16 μM prereduced DCCP-R_{Ch} in 50 mM Hepes-NaOH pH 8.0 containing 2 mM DT, and this solution was used as a blank. After adding 10 μM $DCCP_{Ch}$, reduction was initiated by adding 2 mM Mg-ATP and monitoring the decrease of absorption at 420 nm, indicating the reduction of the DCC from $DCCP_{Ch}$. The time-dependent absorption was fitted to a single exponential equation with Grafit5 (6).

Isothermal Titration Calorimetry. Isothermal titration calorimetry (ITC) measurements were performed using a MicroCal VP-ITC at 25 °C installed in an anoxic glove box (Labstar workstation, MBRAUN) with an atmosphere of N_2 containing less than 0.5 ppm of O_2. $DCCP_{Ch}$ (0.05 mM) in the cell was titrated with 4 mM CoA from the syringe.

Acetylene and Ethylene Reduction Activities. Acetylene (C_2H_2, 99.5%), ethylene (C_2H_4, 99.7%), and ethane (C_2H_2, 99.95%) were purchased from Air-Liquide GmbH, with the highest purity. The reaction mixture for acetylene reduction was prepared in calibrated reaction tubes (overall volume 7 mL) sealed with butyl septum (10-mm thickness) and a screw cap, containing 40% (vol/vol) acetylene in N_2 gas atmosphere. The reaction solution contained 9.5 μM $DCCP_{Ch}$, 20 mM phosphocreatine (PC), 20 mM DT, 0.1 mg/mL creatine phosphokinase (CPK), 40 μM DCCP-R_{Ch} (fourfold molar excess to $DCCP_{Ch}$) in 1 mL with buffer of 50 mM Hepes pH 8.0. Acetylene reduction was initiated by injecting acetylene gas after removal of corresponding volume of N_2 atmosphere in the reaction tube using a gas-tight pressure-lock syringe. The same reaction conditions were used to determine ethylene reduction activity except that 40% (vol/vol) ethylene was used instead of acetylene. Reactions were performed at different temperatures in a shaking water-bath. The reaction was monitored by sampling the gas phase and determine a progress curve or terminated after 30 min by adding 0.25 mL of 0.5 M EDTA.

At every time point 50 μL of gaseous headspace were taken and injected with a gas-tight Hamilton syringe into the gas chromatography (GC)/mass spectrometry (MS)-QP2010 ultra equipped with a Carboxene-1010 PLOT column (30-m × 0.53-mm inner diameter; Shimadzu Europa) using helium as carrier gas. A split ratio of 10 was used. The injection temperature was set to 225 °C, and the column oven temperature was set to 140 °C. Gas components were separated using a temperature gradient. After an initial isocratic temperature at 140 °C for 2.2 min, the temperature was ramped up to 225 °C with a linear velocity of 24 °C/min and kept for 2 min. The MS unit was tuned using perfluorotributylamine and detected gas samples by SIM mode (m/z = 28 for C_2H_4 and m/z = 30 for C_2H_6). The standard curve with high linearity was created by using ethylene diluted with nitrogen in a Hungate tube and its mass was calculated using the gas law relationship (7).

To determine the temperature-dependency of acetylene reduction by $DCCP_{Ch}$, all reactions at the different temperatures were stopped after 30 min, except for reactions at 45 and 50 °C, which were stopped after 20 and 5 min incubation, respectively, due to precipitation of CPK.

The pH dependency of acetylene reduction was determined in 50-mM concentration using following buffers: 2-(*N*-Morpholino)-ethanesulfonic acid (Mes) for pH 6.0, 3-(*N*-Morpholino)-propanesulfonic acid (Mops) for pH 7.0, *N*-(2-Hydroxyethyl)-piperazine-N′-ethanesulfonic acid (Hepes) for pH 8.0, Tris(hydroxymethyl)-aminomethane (Tris) for pH 9.0, 3-(Cyclohexylamino)-propanesulfonic acid (CAPS) for pH 10.0.

Inhibition of Acetylene Reduction. All soluble inhibitors (KCN, NH_2OH, N_3^-, and N_2H_4) were tested in this study by adding 10 mM (final concentration) into the reaction solution containing the same components as in the acetylene reduction reaction. To test inhibition by N_2 gas, activities were compared with a He atmosphere with 40% acetylene. For CO or H_2 as potential inhibitors of acetylene reduction, the N_2 atmosphere of the reaction tube was immediately replaced by CO or H_2 by purging 5 min and after which 40% (vol/vol) of acetylene was added. Reactions were initiated by adding Mg-ATP at 35 °C and terminated by adding 0.25 mL 0.5 M EDTA after 30 min. The gas samples were analyzed by GC/MS, as described above. To test reversibility of CO inhibition, the CO-inhibited sample was freed of CO at a Schlenk line using N_2 gas (n = 5) and 40% (vol/vol) of acetylene was added to initiate the reaction. Every inhibition assay was measured at least twice.

Ammonia Detection. Ammonia was quantified using a fluorescence method described previously (8) with some modifications (9). Forty millimolar each of a nitrogenous substrate (KCN, N_3^- and N_2H_4) was added to 3 mL of reaction solution containing the same components as in the acetylene reduction assay. The reaction was initiated by adding Mg-ATP and incubated at 35 °C. At specific time points, 0.5-mL aliquots of the reaction were terminated by addition of 150 μL of 0.5 M EDTA and filtrated by a concentrator with a molecular cut-off of 5 kDa. Next, 50 μL of flow-through from the filtration was used to form the ammonia-*o*-phthalaldehyde fluorescent product, which was detected by fluorimetry at $\lambda_{excitation}/\lambda_{emission}$ of 410 nm/472 nm using the fluorescence spectrophotometer FP-6500 equipped with a temperature controller ETC-273T (JASCO). Ammonia released from the substrate was quantified using a standard curve generated using NH_4Cl. At each reaction, the quantity of ammonia was subtracted from reaction at t_0. All experiments were conducted in the dark.

Crystallization and Crystal Treatment. As-isolated $DCCP_{Ch}$ (18 mg/mL) was crystallized using the hanging-drop vapor diffusion method in a condition containing 10–13% (wt/vol) PEG 8000, 0.1 M Na-citrate pH 5.0 in the presence of 2 mM DT. Crystals were harvested and flash-cooled in the reservoir solution supplemented with 30% (vol/vol) glycerol as a cryoprotectant. For xenon soaking, a crystal harvested in the cryo buffer was pressurized under 40 bars of xenon for 5 min and subsequently cryo-cooled after slowly releasing the pressure.

Data Collection and Structure Refinements. All diffraction datasets were collected at 100 K at Beamline 14.1 (BESSY, Berlin, Germany) (10). Anomalous diffraction datasets were collected at the specified wavelength shown in Table S1. The datasets were integrated and scaled using XDSAPP (11). The structure of $DCCP_{Ch}$ was solved by SAD phasing using anomalous diffraction data collected at the Fe K-edge using PHENIX (12). Model

building was carried out with COOT (13). Iterative refinement cycles were performed with PHENIX and refmac in CCP4 (12, 14). Statistics of data collection and refinements are reported in Table S1. Restraints for bond lengths and angles of the iron–sulfur cluster in $DCCP_{Ch}$ used at the initial refinement were released in the final refinement cycle.

1. Nakamura M, Saeki K, Takahashi Y (1999) Hyperproduction of recombinant ferredoxins in *Escherichia coli* by coexpression of the *ORF1-ORF2-iscS-iscU-iscA-hscB-hscA-fdx-ORF3* gene cluster. *J Biochem* 126:10–18.
2. Bradford MM (1976) A rapid and sensitive method for the quantitation of microgram quantities of protein utilizing the principle of protein-dye binding. *Anal Biochem* 72:248–254.
3. Gerlt JA, et al. (2015) Enzyme function initiative-enzyme similarity tool (EFI-EST): A web tool for generating protein sequence similarity networks. *Biochim Biophys Acta* 1854:1019–1037.
4. Shannon P, et al. (2003) Cytoscape: A software environment for integrated models of biomolecular interaction networks. *Genome Res* 13:2498–2504.
5. Lanzetta PA, Alvarez LJ, Reinach PS, Candia OA (1979) An improved assay for nanomole amounts of inorganic phosphate. *Anal Biochem* 100:95–97.
6. Leatherbarrow RJ (2001) *GraFit Version 5* (Erithacus Software, Horley, UK).
7. Somasegaran P, Hoben HJ (1994) *Handbook for Rhizobia* (Springer, New York).
8. Corbin JL (1984) Liquid chromatographic-fluorescence determination of ammonia from nitrogenase reactions: A 2-min assay. *Appl Environ Microbiol* 47:1027–1030.
9. Spatzal T, Perez KA, Howard JB, Rees DC (2015) Catalysis-dependent selenium incorporation and migration in the nitrogenase active site iron-molybdenum cofactor. *eLife* 4:e11620.
10. Mueller U, et al. (2015) The macromolecular crystallography beamlines at BESSY II of the Helmholtz-Zentrum Berlin: Current status and perspectives. *Eur Phys J Plus* 130: 141.
11. Krug M, Weiss MS, Heinemann U, Mueller U (2012) XDSAPP: A graphical user interface for the convenient processing of diffraction data using XDS. *J Appl Cryst* 45: 568–572.
12. Adams PD, et al. (2010) PHENIX: A comprehensive Python-based system for macromolecular structure solution. *Acta Crystallogr D Biol Crystallogr* 66:213–221.
13. Emsley P, Lohkamp B, Scott WG, Cowtan K (2010) Features and development of Coot. *Acta Crystallogr D Biol Crystallogr* 66:486–501.
14. Winn MD, et al. (2011) Overview of the CCP4 suite and current developments. *Acta Crystallogr D Biol Crystallogr* 67:235–242.

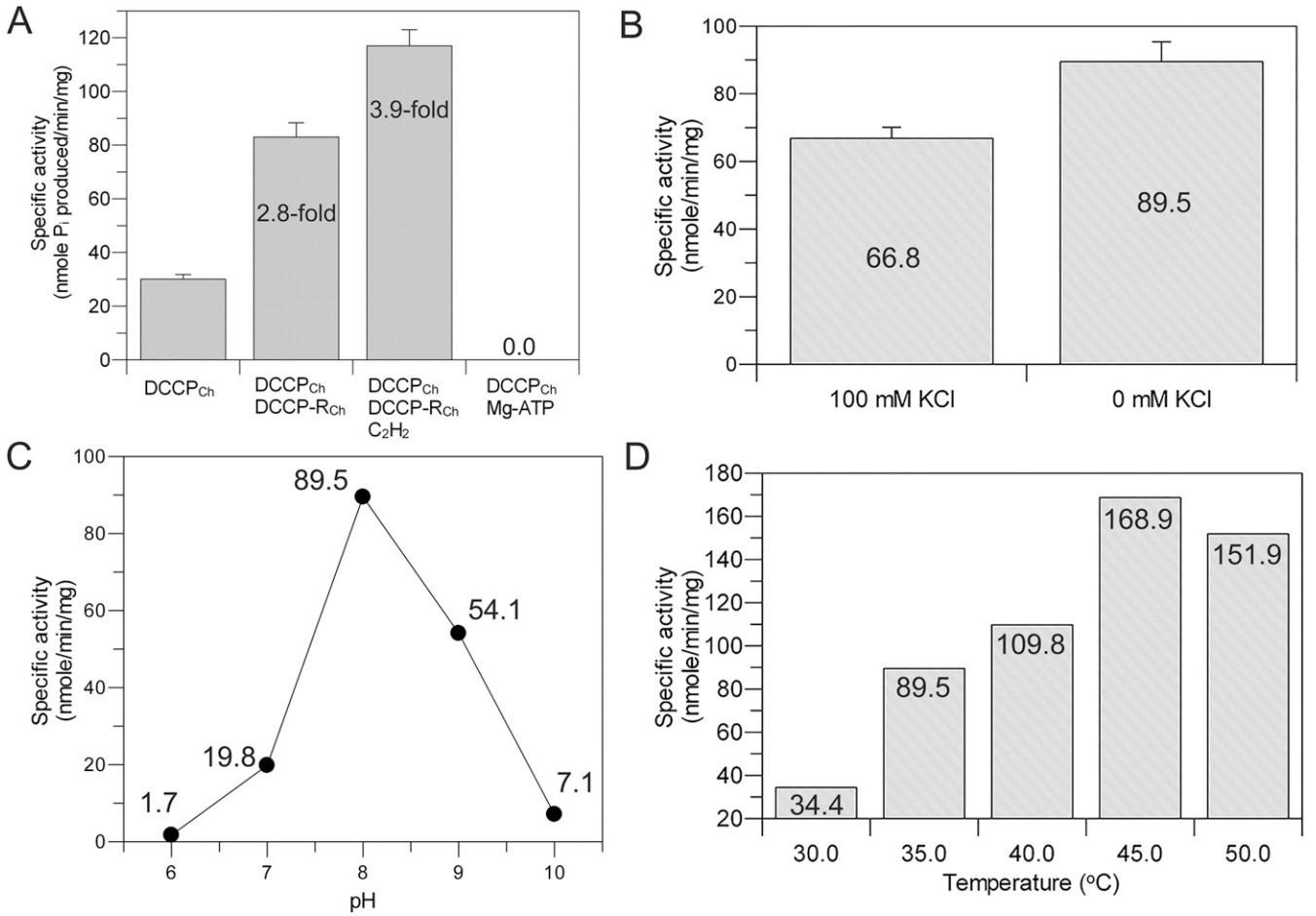

Fig. S1. ATPase and acetylene reduction activity. (*A*) ATPase activity of DCCP-R_{Ch}. Reactions with both proteins contained oxidized $DCCP_{Ch}$ and reduced DCCP-R_{Ch}. Error bars are derived from at least three independent measurements ($n = 3$). The control measurement contained oxidized $DCCP_{Ch}$ and Mg-ATP. (*B*) KCl-dependence of acetylene reduction. Activity was determined with and without 100 mM KCl. (*C*) Temperature-dependence of acetylene reduction. Activities at 30 °C, 35 °C, and 40 °C were assessed after stopping the reaction after 30 min, while at 45 °C and 50 °C activities were determined after 20 and 5 min, respectively. All assay conditions contained 50 mM Hepes-NaOH pH 8.0. (*D*) pH-dependence of acetylene reduction.

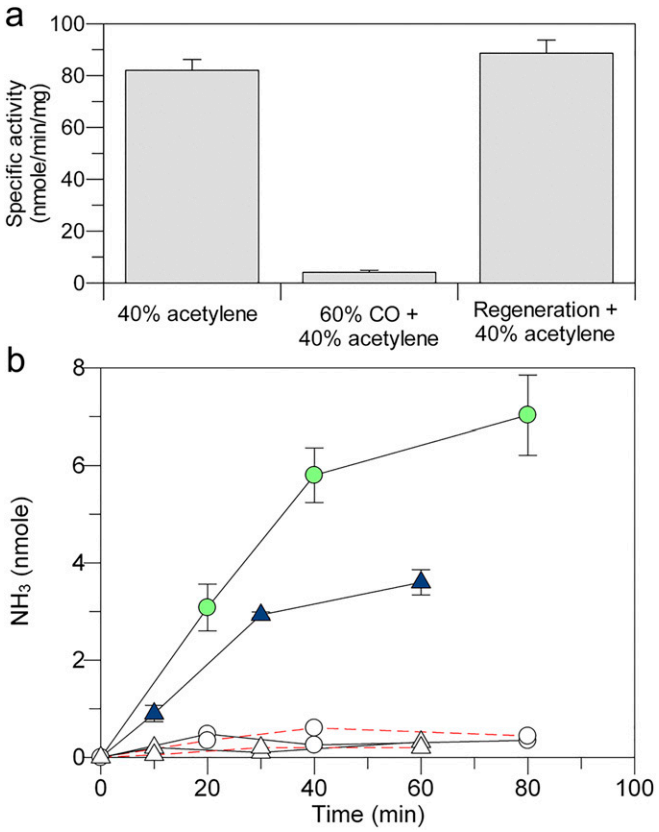

Fig. S2. Inhibition and activities of $DCCP_{Ch}$. (*A*) Reversible inhibition of acetylene reduction by CO. Regeneration indicates that the CO atmosphere was replaced with N_2 gas at a Schlenk line. Activities were determined from three independent measurements. (*B*) Ammonia formation from azide (N_3^-) and hydrazine (N_2H_4) are shown in circles and triangles, respectively ($n = 4$). Amounts of ammonia are based on 50 μL of reaction volumes. Control reactions with azide (empty-circle) and hydrazine (empty-triangle) in the absence of either $DCCP_{Ch}$ (solid-line) or DCCP-R_{Ch} (dotted-line) are shown.

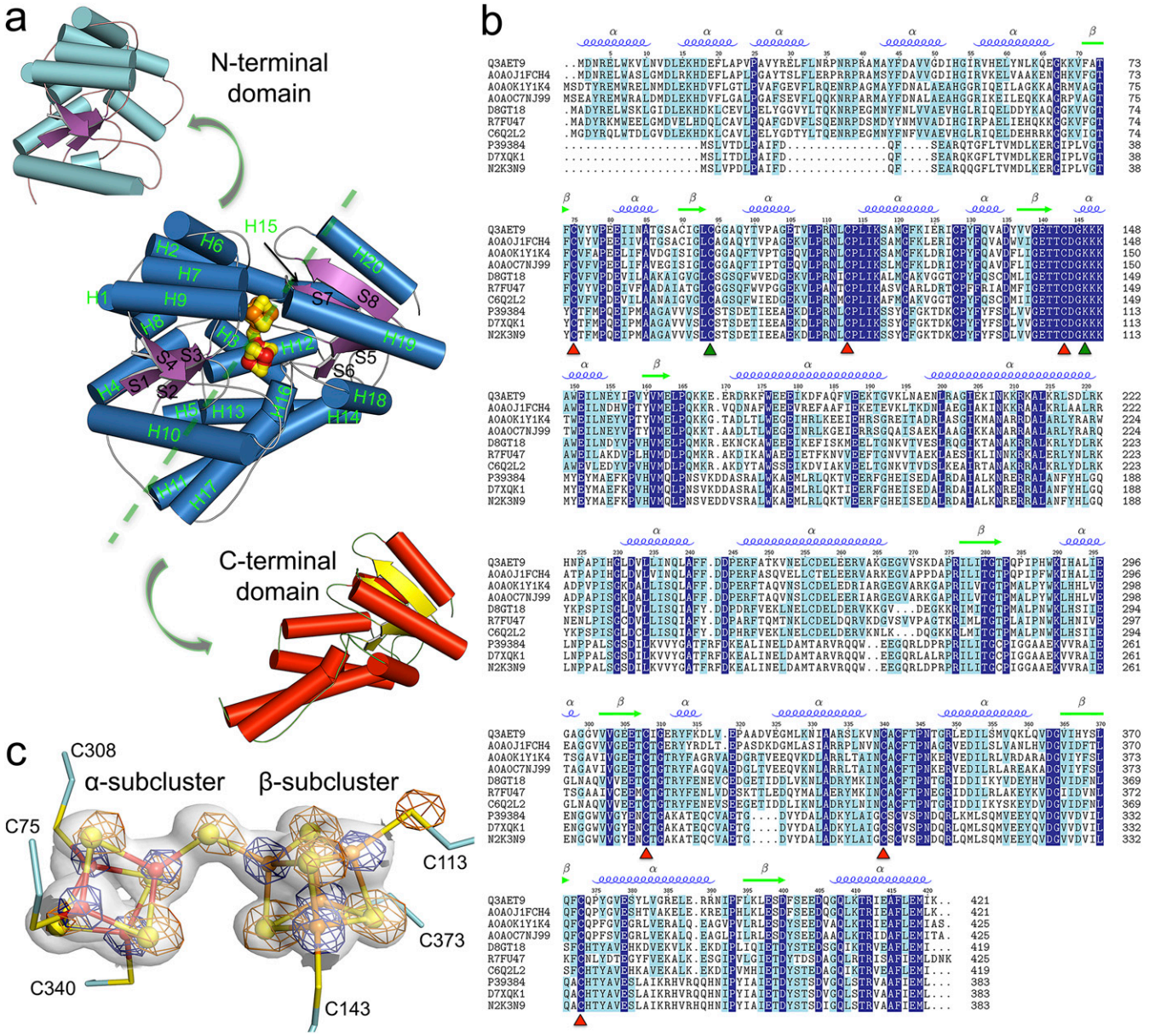

Fig. S3. (*A*) Secondary structure of $DCCP_{Ch}$. H and S indicate α-helix and β-strand, respectively. (*B*) Sequence alignment. Red triangles depict the six conserved cysteine residues coordinating the $[Fe_8S_9]$-cluster. Green triangles indicate an additional, conserved cysteine, and a conserved lysine near the cluster. InterPro accession numbers denote selected sequences with homology to $DCCP_{Ch}$: Q3AET9, *C. hydrogenoformans*; R4KME1, *Desulfotomaculum gibsoniae* DSM 7213; A5D4T6, *Pelotomaculum thermopropionicum* SI; Q2RIK8, *Moorella thermoacetica* ATCC 39073; F7V8C0, *Clostridium* sp. SY8519; P39384, *Escherichia coli* K12; W1AQH3, *Klebsiella pneumoniae* IS22; A0A142GYN5, *Shigella* sp. PAMC 28760. (*C*) Electron density maps. Anomalous difference densities of iron (blue, 18 σ, λ = 1.74 Å) and sulfur (orange, 8 σ, λ = 1.90 Å) atoms are shown as mesh. An $F_o - F_c$ omit map is shown with gray surface at 4 σ. For comparison, the anomalous scattering contribution of S^{γ}-Cys^{113} is shown as orange mesh.

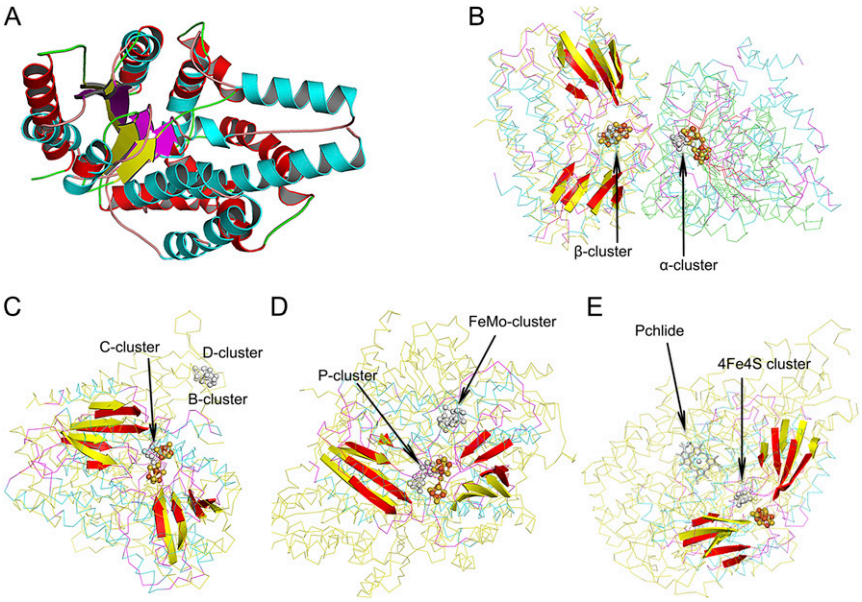

Fig. S4. Superposition of structures. (*A*) Superposed N-terminal (cyan helices and pink strands) and C-terminal domain (red helices and yellow strands) of $DCCP_{Ch}$. (*B*) Dimeric $DCCP_{Ch}$ was superposed on the α-subunit (green carbon) and the β-subunit (yellow carbon) of 2-hydroxyisocaproyl-CoA dehydratase (PDB ID code 3O3N; *z*-score: 42.2 and rmsd of 2.2 Å for 366 aligned Cα-atoms with the β-subunit, *z*-score of 31.7 and rmsd of 2.8 Å for 359 aligned Cα-atoms with α-subunit). (*C*) Superposition of one subunit of $DCCP_{Ch}$ with one subunit of Ni,Fe-CODH (yellow carbon from PDB ID code of 1JQK, *z*-score of 5.3 and rmsd of 4.8 Å for 167 aligned Cα-atoms). (*D*) One subunit of $DCCP_{Ch}$ was superposed on Mo,Fe-nitrogenase (yellow carbon from PDB ID code 2AFK; *z*-score of 4.1 and rmsd of 5.5 Å for 113 aligned Cα-atoms). (*E*) Superposition of monomeric $DCCP_{Ch}$ on catalytic unit (BN subunits) of DPOR (PDB ID code 2YNM; rmsd of 5.4 Å for 183 aligned Cα-atoms). Gray spheres indicate metal clusters of the superimposed structures. Superimpositions were calculated with COOT (1) using the secondary structure matching (SSM) algorithm without further adjustments. For clarity, the central β-sheet of the Rossmann-fold is presented as cartoon.

1. Emsley P, Lohkamp B, Scott WG, Cowtan K (2010) Features and development of Coot. *Acta Crystallogr D Biol Crystallogr* 66:486–501.

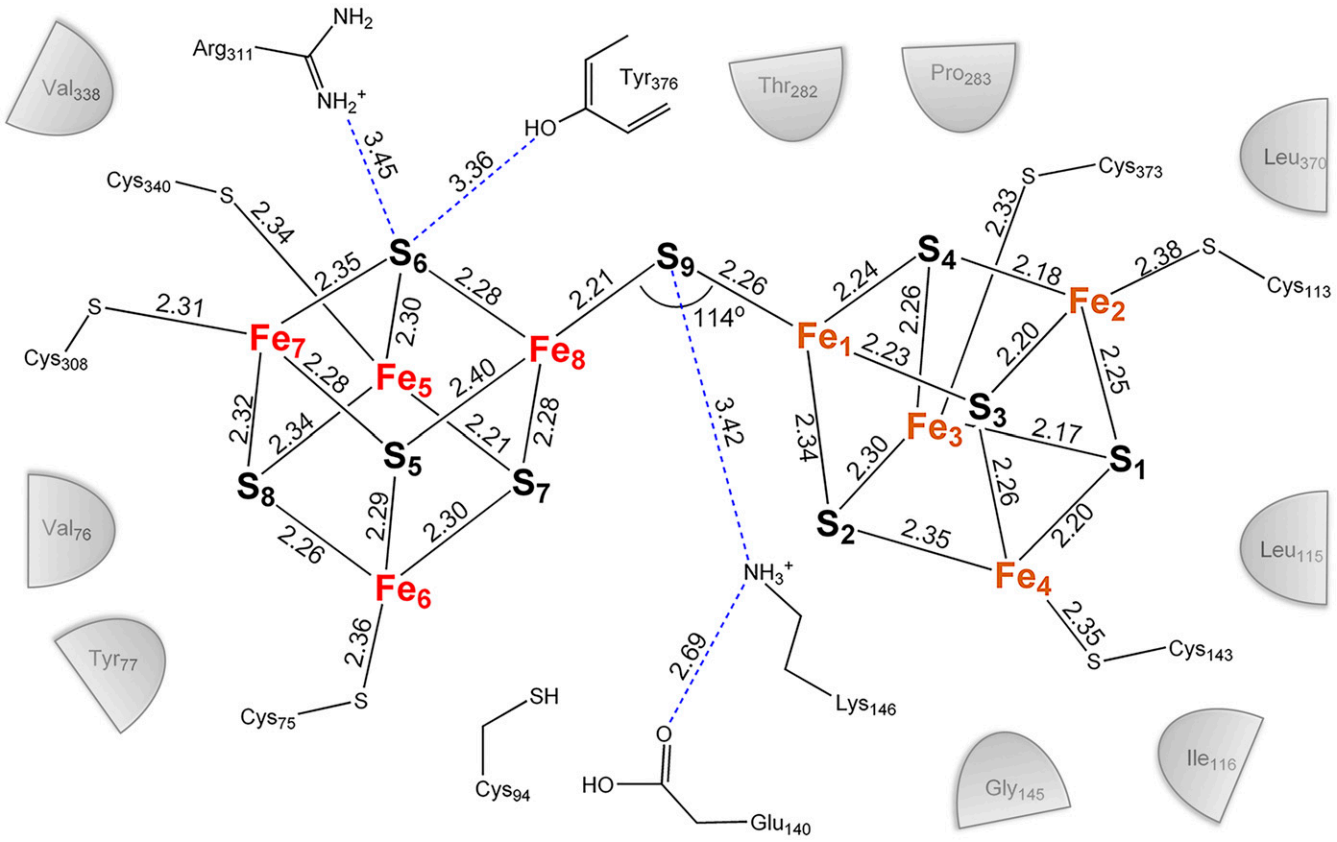

Fig. S5. Schematic drawing of the DCC with bond lengths and its environment. Iron atoms are shown in red for the α-subcluster and orange for β-subcluster, as in Fig. 4. Possible H-bonding interactions are shown as blue dotted-lines. Residues with hydrophobic side chains pointing to the DCC are depicted in gray. All residues within a sphere of 5 Å around the clusters are depicted.

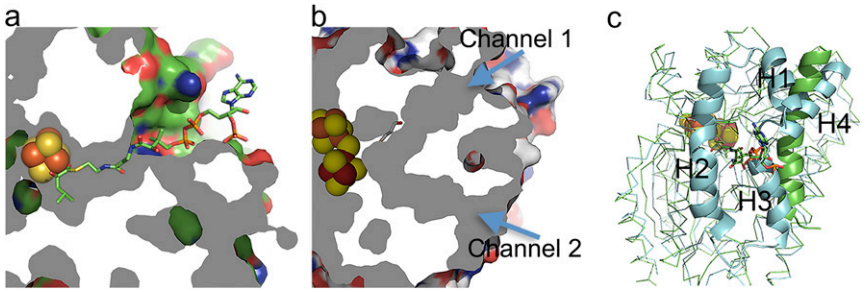

Fig. S6. Comparing the structures of $DCCP_{Ch}$ and 2-hydroxyisocaproyl-CoA dehydratase. Surface representations of (*A*) the α-subunit of 2-hydroxyisocaproyl-CoA dehydratase (PDB ID code 3O3N) (1) with bound isocaproyl-CoA and (*B*) $DCCP_{Ch}$. Both structures are shown in same orientation and scale after superimposition (rmsd of 2.49 Å). Spheres indicate iron–sulfur clusters. (*C*) Superimposed structures of 2-hydroxyisocaproyl-CoA dehydratase (green) and $DCCP_{Ch}$ (cyan). The main differences are found in the N-terminal regions, here shown as cartoons. Helix numbering of $DCCP_{Ch}$ is same as in Fig. S4*A*.

1. Knauer SH, Buckel W, Dobbek H (2011) Structural basis for reductive radical formation and electron recycling in (R)-2-hydroxyisocaproyl-CoA dehydratase. *J Am Chem Soc* 133:4342–4347.

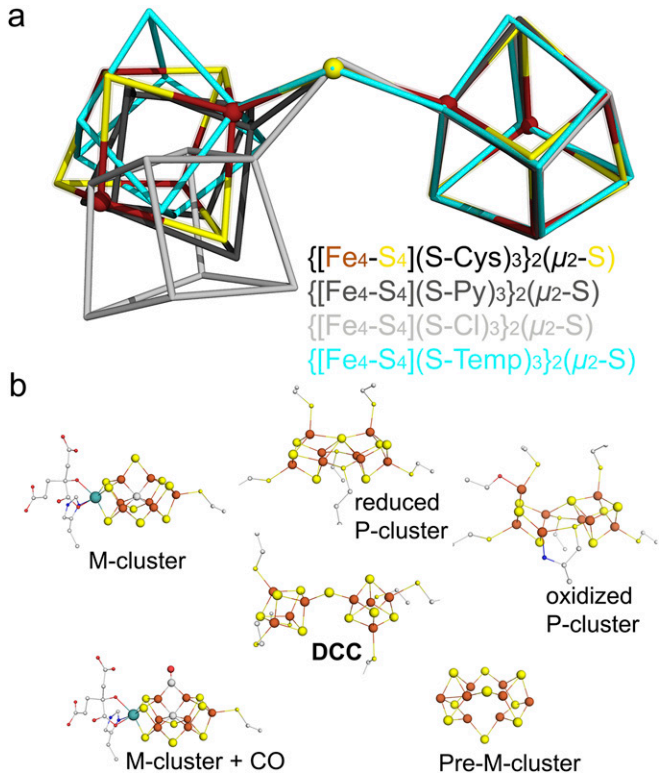

Fig. S7. DCC in comparison with complex Fe/S clusters in inorganic chemistry and biology. (*A*) Sulfide-bridged double cubane [Fe_4S_4] clusters. $DCCP_{Ch}$ cluster is shown in element colors. {[Fe_4S_4](S-Py)$_3$}$_2$(μ_2-S), {[Fe_4S_4](S-Cl)$_3$}$_2$(μ_2-S) and {[Fe_4S_4](S-Temp)$_3$}$_2$(μ_2-S) are from refs. 1–3. The DCC of $DCCP_{Ch}$ has a dihedral angle of 25° between planes formed by Fe^1-Fe^3-S^9 and Fe^8-Fe^6-S^9 (shown as spheres), placing S^5-Fe^8-S^9-Fe^1-S^4 in one line. The Fe^8-μ_2-S^9-Fe^1 bridge forms an angle of 114° with bond lengths of 2.21 and 2.26 Å for Fe^8-μ_2-S^9 and μ_2-S^9-Fe^1, respectively. This is slightly shorter than the average Fe-S_γ-Cys bond lengths of 2.35 Å. Mean Fe-S bond lengths in the clusters are 2.27 Å, while mean Fe-Fe distances in the clusters are 2.70 Å. Angles between μ_2-S^9-Fe^8-S^7 and μ_2-S^9-Fe^1-S^2 are 117° and 115°, respectively, which are comparable to the μ_3-S-Fe-S_γ-Cys angles (100°–124°). (*B*) Comparison of the DCC of $DCCP_{Ch}$ to nitrogenase-related clusters: M-cluster (FeMoco), reduced P-cluster, precursor of M-cluster, oxidized P-cluster and M-cluster + CO are derived from PDB IDs codes 3U7Q (4), 2MIN (5), 3PDI (6), 4TKV (7), respectively.

1. Challen PR, Koo SM, Dunham WR (1990) New μ_2-S^{2-}-coupled, singly bridged double cubane with the $[(Fe_4S_4Cl_3)_2S]^{4-}$ core. The stepwise synthesis and structural characterization of (n-$Bu_4N)_2(Ph_4P)_2$. *J Am Chem Soc* 112:2455–2456.
2. Terada T, et al. (2012) Tridentate thiolate ligands: Application to the synthesis of the site-differentiated [4Fe-4S] cluster having a hydrosulfide ligand at the unique iron center. *Chem Asian J* 7:920–929.
3. Gerlach DL, Coucouvanis D, Kampf J, Lehnert N (2013) Isolation and characterization of single and sulfide-bridged double [4Fe-4S] cubane clusters with 4-pyridinethiolato ligands. *Eur J Inorg Chem* 2013:5253–5264.
4. Spatzal T, et al. (2011) Evidence for interstitial carbon in nitrogenase FeMo cofactor. *Science* 334:940.
5. Peters JW, et al. (1997) Redox-dependent structural changes in the nitrogenase P-cluster. *Biochemistry* 36:1181–1187.
6. Kaiser JT, Hu Y, Wiig JA, Rees DC, Ribbe MW (2011) Structure of precursor-bound NifEN: A nitrogenase FeMo cofactor maturase/insertase. *Science* 331:91–94.
7. Spatzal T, Perez KA, Einsle O, Howard JB, Rees DC (2014) Ligand binding to the FeMo-cofactor: Structures of CO-bound and reactivated nitrogenase. *Science* 345:1620–1623.

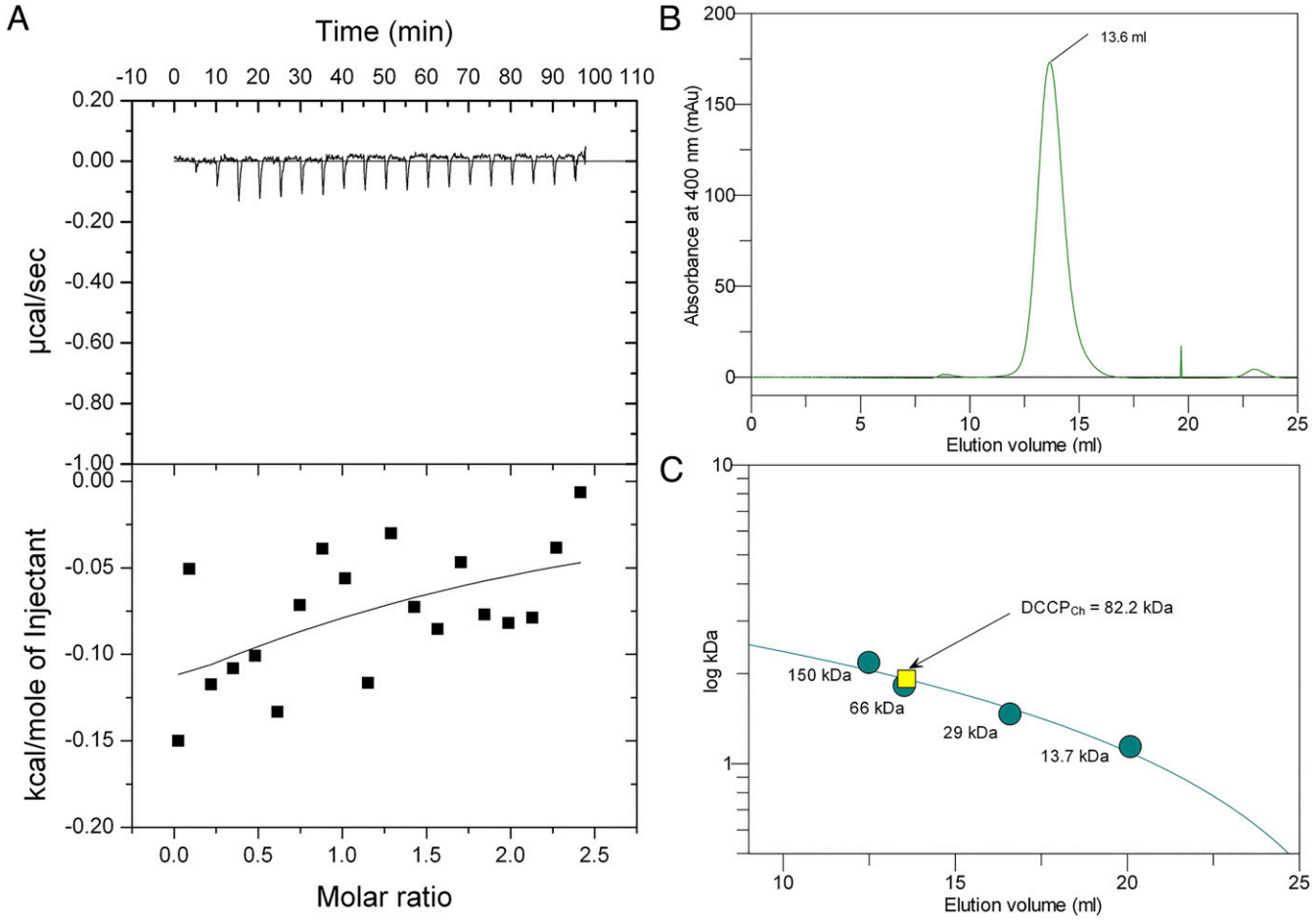

Fig. S8. ITC and size-exclusion chromatography of $DCCP_{Ch}$. (*A*) ITC-thermogram of titrating $DCCP_{Ch}$ with CoA. 50 µM $DCCP_{Ch}$ in the cell was titrated with 4 mM CoA. (*B*) Size-exclusion chromatography of $DCCP_{Ch}$. The elution profile was recorded using the absorbance at 400 nm. (*C*) Molecular weight determination of $DCCP_{Ch}$. Molecular size markers were used to generate a standard curve (cyan circle): alcohol dehydrogenase (150 kDa), albumin (66 kDa), carbonic anhydrase (29 kDa), and ribonuclease (13.7 kDa). A regression curve is shown as cyan solid line. A yellow square indicates the elution volume of $DCCP_{Ch}$.

Table S1. Data collection and refinement statistics

Data parameter	Native	Fe-HighE	S-HighE	Xe
Data collection				
Wavelength, Å	0.9184	1.74	1.9	1.9
Space group	$P6_522$	$P6_522$	$P6_522$	$P6_522$
Cell dimensions				
a, *b*, *c*, Å	80.59, 80.59, 217.43	80.38, 80.38, 216.42	80.50, 80.50, 216.93	80.89, 80.89, 217.31
Resolution, Å	42.9–1.63	42.8–1.94	50–2.2	43.5–2.14
R_{merge}*	7.0 (68.7)	6.2 (17.0)	9.4 (27.2)	5.5 (34.2)
I/σ *I**	13.9 (2.4)	18.3 (3.4)	37.2 (7.9)	17.42 (3.51)
Completeness, %*	98.8 (92.2)	98.7 (92.8)	95.4 (74.6)	99.8 (98.7)
Redundancy*	7.0 (7.0)	6.1 (3.1)	18.2 (8.7)	5.4 (4.1)
Refinement				
Resolution, Å	42.9–1.63			
No. reflections	51,968			
R_{work}/R_{free}	17.2/21.3			
No. atoms				
Protein	3,416			
Ligand/ion	42			
Water	443			
B-factors				
Protein	29.9			
Ligand/ion	31.7			
Water	37.8			
Rmsd				
Bond lengths, Å	0.112			
Bond angles, °	1.202			

*Values in parentheses are for highest-resolution shell.